Functionalized Graphene Oxide as a Nanocarrier in a Multienzyme Labeling Amplification Strategy for Ultrasensitive Electrochemical Immunoassay of Phosphorylated p53 (S392)

ARTICLE *in* ANALYTICAL CHEMISTRY · FEBRUARY 2011

Impact Factor: 5.64 · DOI: 10.1021/ac101715s · Source: PubMed

6 AUTHORS, INCLUDING:

Dan Du
Washington State University
128 PUBLICATIONS **3,744** CITATIONS
SEE PROFILE

Jun Wang
Nanjing University of Posts and Telecommu…
355 PUBLICATIONS **11,624** CITATIONS
SEE PROFILE

Mark H Engelhard
Pacific Northwest National Laboratory
381 PUBLICATIONS **11,983** CITATIONS
SEE PROFILE

Yuehe Lin
Washington State University
363 PUBLICATIONS **21,408** CITATIONS
SEE PROFILE

analytical chemistry

ARTICLE

pubs.acs.org/ac

Functionalized Graphene Oxide as a Nanocarrier in a Multienzyme Labeling Amplification Strategy for Ultrasensitive Electrochemical Immunoassay of Phosphorylated p53 (S392)

Dan Du,[†,‡] Limin Wang,[‡] Yuyan Shao,[‡] Jun Wang,[‡] Mark H. Engelhard,[‡] and Yuehe Lin*[,‡]

[†]Key Laboratory of Pesticide and Chemical Biology of Ministry of Education, College of Chemistry, Central China Normal University, Wuhan 430079, People's Republic of China

[‡]Pacific Northwest National Laboratory, Richland, Washington 99352, United States

ABSTRACT: P53 phosphorylation plays an important role in many biological processes and might be used as a potential biomarker in clinical diagnoses. We report a new electrochemical immunosensor for ultrasensitive detection of phosphorylated p53 at Ser392 (phospho-p53^{392}) based on graphene oxide (GO) as a nanocarrier in a multienzyme amplification strategy. Greatly enhanced sensitivity was achieved by using the bioconjugates featuring horseradish peroxidase (HRP) and p53^{392} signal antibody (p53^{392}Ab$_2$) linked to functionalized GO (HRP−p53^{392}Ab$_2$−GO) at a high ratio of HRP/p53^{392}Ab$_2$. After a sandwich immunoreaction, the HRP−p53^{392}Ab$_2$−GO captured onto the electrode surface produced an amplified electrocatalytic response by the reduction of enzymatically oxidized thionine in the presence of hydrogen peroxide. The increase of response current was proportional to the phospho-p53^{392} concentration in the range of 0.02−2 nM with the detection limit of 0.01 nM, which was 10-fold lower than that of the traditional sandwich electrochemical measurement for p53^{392}. The amplified immunoassay developed in this work shows acceptable stability and reproducibility, and the assay results for phospho-p53^{392} spiked in human plasma also show good recovery (92−103.8%). This simple and low-cost immunosensor shows great promise for detection of other phosphorylated proteins and clinical applications.

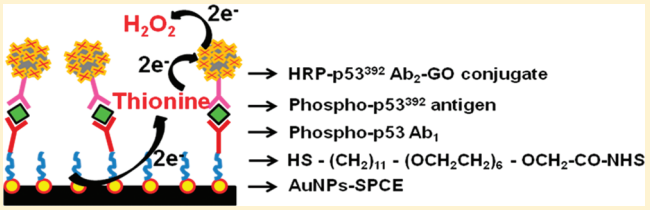

The p53 protein, a well-known tumor suppressor and a transcription factor, plays an important role in controlling cell growth and modulating DNA repair processes.[1−3] Loss of p53 function results in an induction of tumors and gene mutation, which is caused by the conformational changes in p53 protein structure.[4,5] It has been reported that p53 can be stabilized and accumulated in the tumor cell nucleus as the result of p53 phosphorylation. There are a few data concerning the measurement of p53 protein phosphorylation in tumor tissues.[6−12] Some results have shown a clinical implication of p53 phosphorylation in human cancers.[10,11] For example, Bar's group evaluated expression of p53 protein phosphorylated at serine 20 (Ser20) and serine 392 (Ser392) involved in ovarian neoplasms.[7] Yap et al. suggested that p53-Ser392 phosphorylation may regulate the oncogenic function of mutant forms of p53 protein in breast cancer.[10] Other authors think that p53 phosphorylated at Ser392 could be considered an independent prognostic factor in advanced human esophageal squamous cell carcinomas (ESCCs).[11] A recent study reported that p53 phosphorylated on serine 15 might be used as a potential biomarker of γ-radiation exposure since the phosphorylation is dose-dependent.[13] On the basis of these results, quantitative determination of phosphorylated p53 is of great significance in clinical research and early diagnosis of cancers.

Thus far, the most popular method for measuring phosphorylated p53 protein is enzyme-linked immunosorbant assay (ELISA).[13,14] Although ELISA is a powerful tool for the detection of antigens and several commercial detection kits are available with very low detection limits, it involves several incubation and washing steps followed by spectrophotometric detection using a chromogenic substrate. In addition, ELISA needs more expensive instruments and is lab-oriented. In comparison with the ELISA method, electrochemical immunoassay has attracted considerable interest because of its intrinsic advantages such as portability, low cost, high sensitivity, and low power requirement. Several electrochemical immunosensors have been developed and extensively applied to the determination of tumor markers.[15−17] In order to meet the increasing demand for early and ultrasensitive detection of biomarkers, various signal amplification technologies using nanomaterials have been developed: (1) Metal and semiconductor nanoparticles are directly used as electroactive labels to amplify the electrochemical responses.[18,19] (2) Nanoparticles are used as carriers to load a large amount of electroactive species, such as ferrocene, to amplify the detection signal.[20−23] (3) One of the most popular strategies is enzyme-functionalized nanoparticles used as labels to enhance the detection sensitivity by loading a large amount of enzyme toward an individual sandwich immunological reaction event. Various nanomaterials have been used as carriers to load enzymes and antibodies including carbon nanotubes (CNTs),[24,25] carbon nanospheres,[26] gold nanoparticles,[27] silica

Received: June 29, 2010
Accepted: December 9, 2010
Published: January 6, 2011

nanoparticles,[28] and carboxylated magnetic beads.[29] For example, Rusling's group[24,25] has achieved greatly enhanced sensitivity using bioconjugates featuring horseradish peroxidase (HRP) labels and signal antibodies linked to CNTs for immunodetection of the prostate-specific antigen and interleukin-6, respectively. Lai et al.[27] designed a novel tracer by one-pot assembly of glucose oxidase and antibodies on gold nanoparticles for ultrasensitive multiplexed measurement of tumor markers. Our group has developed a sensitive immunosensor for α-fetoprotein detection based on carbon nanosphere/HRP labeling.[26]

The interesting physical properties of graphene, a novel one-atom-thick and two-dimensional graphitic carbon system, have led to much excitement in recent years and potential applications in sensors, nanoelectronic devices, and nanocomposite materials.[30−37] Recently, a few research groups have explored biological applications of graphene and graphene oxide (GO) for cellular imaging and drug delivery.[38−41] They found that the loading ratio (the weight ratio of loaded drug to carriers) of GO could reach 200%, much higher than that of other nanocarriers such as nanoparticles that usually have a loading ratio less than 100%. Their work demonstrates that GO derivatives can be used as efficient nanocarriers due to their advantages of large surface area, good biocompatibility, and physiological stability. However, the controlled loading of enzymes and antibodies to be designed as a tracer in immunosensing detection remains relatively unexplored. In comparison to other carbon materials, GO, with high-density carboxyl functional groups, is much easier to facilitate biomolecules binding via EDC chemistry.[40,41]

Our present work is motivated by the promising applications of enzyme-functionalized nanoparticles in signal amplification for ultrasensitive detection of biomarkers. Herein, the GO is prepared by oxidizing graphite according to the modified Hummer's method[42−44] and employed as a nanocarrier for enzyme and antibody coimmobilization. Greatly amplified sensitivity is achieved by using the bioconjugates featuring HRP and phospho-p53^{392} signal antibody (p53^{392}Ab$_2$) linked to functionalized GO via amidization to the carboxylate groups of GO at a high HRP/p53^{392}Ab$_2$ ratio. For immunosensor fabrication, a gold nanoparticles (AuNPs) modified screen-printed carbon electrode (SPCE) is used as sensor platform to self-assemble a layer of *N*-hydroxysuccinimide-activated hexa(ethylene glycol) undecane thiol (NHS) for primary antibodies attachment. Upon the completion of sandwich immunoreactions, the HRP−p53^{392}Ab$_2$−GO conjugate is captured onto the electrode surface. Electrochemical detection of enzymatic products is performed in the presence of hydrogen peroxide (H_2O_2) and thionine (Scheme 1). Results demonstrated that the immunosensor based on this amplification strategy has good dynamic range from 0.02 to 2 nM and low detection limit (0.01 nM) for phosphorylated p53-S392 (phospho-p53^{392}). It shows great promise for application in biomedical research, clinical diagnosis, and screening radiation exposure.

Scheme 1. Schematic Illustration of the Multienzyme Labeling Amplification Strategy Using HRP−p53^{392}Ab$_2$−GO Conjugate

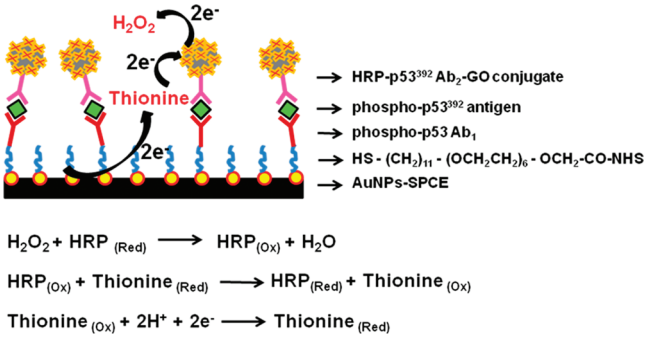

EXPERIMENTAL METHODS

Reagents and Materials. The human phospho-p53 (S392) ELISA kit including phospho-p53^{392} capture antibody, phospho-p53^{392} antigen, biotin−phospho-p53^{392} detection antibody, and streptavidin−HRP, the human phospho-p53 (S15) ELISA kit, and the human phospho-p53 (S46) ELISA kit were purchased from R&D Systems Inc. Graphite powder (<45 mm), bovine serum albumin (BSA), Triton X-100, Tween-20, 1-ethyl-3-(3-dimethylaminopropyl) carbodiimide hydrochloride (EDC), *N*-hydroxysuccinimide (NHS), sodium chloroacetate ($ClCH_2COONa$), thionine, 3,3′,5,5′-tetramethylbenzidine (TMB), phosphate buffer saline (PBS), and 2-(*N*-morpholino)ethanesulfonic acid (MES) were acquired from Sigma-Aldrich. *N*-Hydroxysuccinimide-activated hexa(ethylene glycol) undecane thiol (NHS) was obtained from Nano-Science Instrument Inc.

Apparatus. Electrochemical experiments, including cyclic voltammetry and square wave voltammetry (SWV), were performed with an electrochemical analyzer CHI 660A (CH Instruments, Austin, TX) connected to a personal computer. Disposable gold nanoparticles modified screen-printed carbon electrodes (AuNPs−SPCE) were purchased from Dropsens Inc. A sensor connector (Dropsens Inc.) was used to connect the disposable AuNPs−SPCE with the CHI electrochemical analyzer. Confocal imaging was performed at a Zeiss LSM 710 NLO laser scanning confocal microscope with an upright Zeiss Axioexaminer stand. Transmission electron microscopy (TEM) images were collected with holey carbon TEM grids on a JEOL JSM-2010 TEM microscope operated at 200 kV. X-ray photoelectron spectroscopy (XPS) measurements were taken with a Physical Electronics Quantum 2000 scanning microprobe. X-ray diffraction (XRD) patterns were obtained using a Philips Xpert X-ray diffractometer with Cu Kα radiation at λ = 1.54 Å. UV−vis measurements were carried out at room temperature on a Safire 2 microplate reader (Tecan, Switzerland).

Synthesis of Graphene Oxide. GO was prepared according to our previous study.[44] Typically, 5.0 g of graphite powder was added into 180 mL of concentrated H_2SO_4 and stirred for 1 h. Then 60 mL of fuming HNO_3 was slowly added to the mixture under ice-cooling and stirring. An amount of 25 g of $KMnO_4$ was slowly added under ice-cooling and stirring. The mixed slurry was stirred at room temperature for 120 h. After that, 600 mL of deionized (DI) water was slowly added into the reacted slurry and stirred for 2 h; then 30 mL of 30% H_2O_2 was added, and the slurry immediately turned into a bright yellow solution with bubbling. The resultant solution was stirred for 2 h and then allowed to precipitate for 24 h; after that, the supernatant was decanted. The resultant yellow slurry was centrifuged and then washed in 1000 mL of DI water with 5 mL of HCl (37%) and 3 mL of 30% H_2O_2 added. After stirring for 2 h, the solution was centrifuged and then washed again. This process was repeated three times. After that, the yellow slurry was further washed with 500 mL of DI water until the pH of the washing solution increased to neutral (~6.5) (it took about 500 mL × 12 washes). The remaining dark-yellow solid was dried under vacuum at 40 °C for 48 h and ground to a fine powder. The dry process for GO must be carried out at low temperatures because it slowly decomposes (deoxygenates) above

dx.doi.org/10.1021/ac101715s |*Anal. Chem.* 2011, 83, 746–752

60−80 °C.[45] Then 1.0 mg mL^{-1} GO aqueous solution was placed into an ice bath to carry out strong sonication. The ice bath was changed after each treatment to make sure that sample temperature was below 5 °C. At last, the resultant sample was centrifuged at 12 k rgb for 10 min, and the upper solution was taken for future experiments.

Preparation of HRP−p53^{392}Ab$_2$−GO Conjugate. To convert ester, hydroxyl, and epoxide groups to carboxylic groups, 50 mg of NaOH and 50 mg of ClCH$_2$COONa were added to 1 mL of a 1 mg mL^{-1} GO suspension, followed by bath sonication for 2 h. After these treatments, the resulting product GO−COOH was neutralized with dilute hydrochloric acid and purified by repeated rinsing and centrifugation until the product was well-dispersed in deionized water. Then, the GO−COOH suspension was dialyzed against distilled water for over 48 h to remove any ions. For synthesis of HRP−p53^{392}Ab$_2$−GO conjugate, HRP and p53^{392}Ab$_2$ were attached to carboxylated GO using an EDC/NHS amidization protocol with a reaction mixture of 200/1 HRP/p53^{392}Ab$_2$ molar ratio. Briefly, the GO−COOH was mixed with 400 mM EDC and 100 mM NHS in 1 mL of pH 5.2 MES buffer and activated for 30 min. The mixture was centrifuged at 13 000 rpm for 5 min, and the supernatant was discarded. The buffer wash was repeated to remove excess EDC and NHS. Subsequently, the resulting functionalized mixture was dispersed in 1.0 mL of pH 7.4 PBS and sonicated for 5 min to obtain a homogeneous dispersion. Then, 50 μL of HRP at 1 mg mL^{-1} and 50 μL of p53^{392}Ab$_2$ at 5 μg mL^{-1} were added to the dispersion, and the mixture was stirred overnight at 4 °C. The reaction mixture was washed with PBS and centrifuged at 13 000 rpm for 5 min three times, and the supernatant was discarded. The resulting mixture was redispersed in 1.0 mL of pH 7.4 PBS containing 1% BSA and stored at 4 °C. The HRP−p53^{392}Ab$_2$−GO conjugate is stable and can keep enzyme activity for at least 3 weeks.

Fabrication of the Immunosensor. An amount of 5 μL of 2 mg mL^{-1} *N*-hydroxysuccinimide-activated hexa(ethylene glycol) undecane thiol (NHS) was placed on the AuNPs−SPCE at room temperature for 2 h to form a self-assembled layer. After thoroughly washing with water, the electrode was immediately followed by incubation with 5 μL of 90 μg mL^{-1} phospho-p53^{392} capture antibody (Ab$_1$) in pH 7.4 PBS for 1 h. After washing with 0.05% Tween-20 and PBS buffer, the Ab$_1$/NHS/AuNPs−SPCE was incubated in 3% BSA and PBS solution at 37 °C for 1 h to block excess active groups and nonspecific binding sites on the surface. The electrode was then washed with 0.05% Tween-20 and PBS buffer before use.

Immunoassay Procedure for Detection of Phospho-p53^{392}. A sandwich immunoassay was used for determination of phospho-p53^{392}. (1) The immunosensor, Ab$_1$/NHS/AuNPs−SPCE, was incubated with 5 μL of a different concentration of phospho-p53^{392} standard antigen for 60 min, followed by washing with 0.05% Tween-20 and PBS buffer. (2) Next, the electrode (phospho-p53^{392}/Ab$_1$/NHS/AuNPs−SPCE) was incubated with 5 μL of HRP−p53^{392}-Ab$_2$−GO dispersion for 60 min, followed by washing with 0.05% Tween-20 and PBS buffer to remove the nonspecific adsorption of conjugate. (3) The electrochemical detection was performed in a PBS buffer solution containing 25 μM thionine and 2 mM H$_2$O$_2$.

RESULTS AND DISCUSSION

Preparation and Functionalization of GO Conjugate. We developed a simple and convenient route to prepare HRP−p53^{392}Ab$_2$−GO conjugates, as shown in Scheme 2. Briefly, water-soluble GO was first synthesized by oxidizing graphite according to the modified Hummer's method,[42−44] followed by strong sonication to disperse GO and by centrifugation to remove nondispersed large GO layers. The TEM image provides more detailed morphological information on the resulting GO (Figure 1A). It exhibits the typical wrinkle morphology of GO and is exfoliated into single or very thin layers. Sonication treatment of the GO truncated it from several hundreds of nanometers to less than 500 nm in lateral width, with a size distribution mainly from 300 to 350 nm. Figure 1B shows the microscopy image of GO, and Figure 1C shows its size distribution. Figure 2A shows the XRD patterns of graphite (curve a) and GO (curve b). It can be seen that, after oxidation, the sharp diffraction peak in graphite (2θ = 26.5°, corresponding to the interlayer

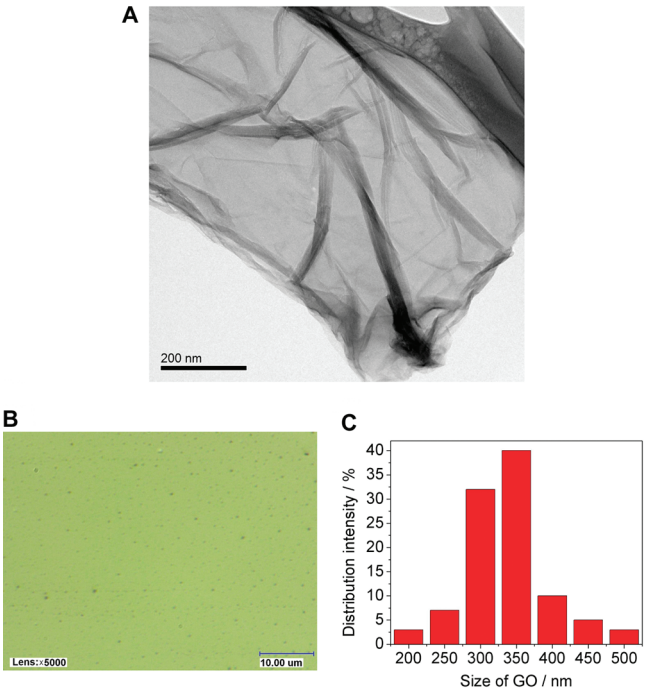

Figure 1. (A) TEM image of the GO; (B) microscope image of synthesized GO; (C) size distribution of GO.

Scheme 2. Schematic Illustration of Preparation of HRP−p53^{392}Ab$_2$−GO Conjugate

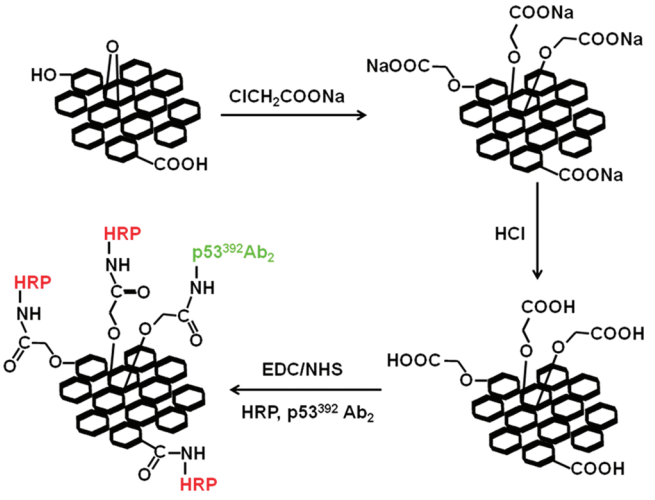

dx.doi.org/10.1021/ac101715s |*Anal. Chem.* 2011, 83, 746–752

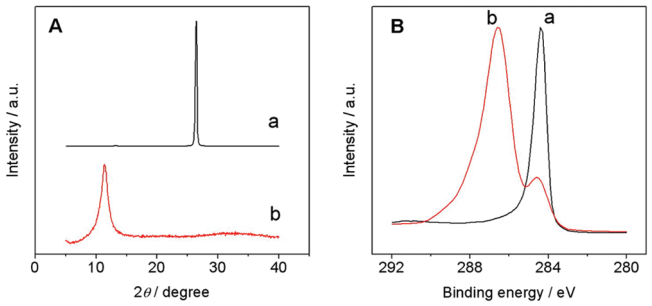

Figure 2. (A) XRD patterns of (a) graphite and (b) GO; (B) XPS measurements of C1s from (a) graphite and (b) GO.

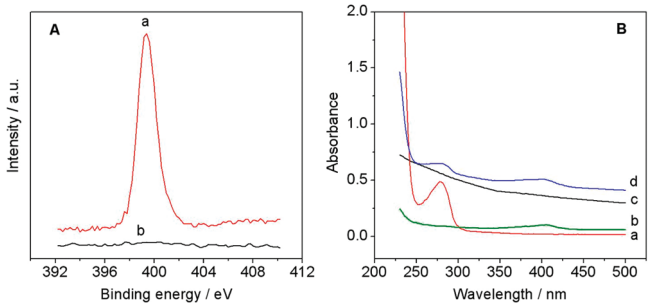

Figure 3. (A) XPS measurements of N1s from (a) HRP−p53^{392}Ab$_2$−GO and (b) GO. (B) UV−vis spectra of (a) p53^{392}Ab$_2$, (b) HRP, (c) GO, and (d) HRP−p53^{392}Ab$_2$−GO conjugate.

distance d = 0.336 nm) disappeared, and a new diffraction peak (2θ = 11.4°, d = 0.777 nm) appeared in GO,[46] indicating the complete oxidation of graphite. This is a prerequisite to successfully exfoliating GO and obtaining single-layer or few-layer graphene sheets.[47] Graphite and GO are further characterized with XPS, and the results are shown in Figure 2B. It can be seen that graphite exhibits a single sharp C1s XPS spectrum centered at 284.3 eV (mainly sp^2 carbon, curve a). GO shows a typical C1s spectrum of heavily oxygenated carbon (curve b). In our previous study, we observed that the relative intensity of oxygen signals was in the order of GO > CNT > graphite, indicating much higher oxygen content in GO than that in CNT and graphite.[44]

There are ester, hydroxyl, and epoxide groups on the GO surface.[38,39] In order to facilitate the binding of enzymes and antibodies to the GO via the EDC/NHS method, it is necessary to convert these groups into carboxyl groups for biomolecule loading. In our strategy, the GO was mixed with ClCH$_2$COONa under strong basic conditions. According to literatures,[38,41] the ester, hydroxyl, and epoxide groups on the GO were converted into carboxyl groups. After removal of the salt and NaOH from the reaction mixture, the precipitated GO−COOH was well-dispersed in distilled water. Conjugation of HRP and p53^{392}Ab$_2$ to GO−COOH was achieved through formation of an amide bond by the reaction between the NH$_2$ groups of the biomolecules and the COOH of GO. As shown in the XPS of Figure 3A, a strong N1s binding energy at 399.6 eV was observed on the HRP−p53^{392}Ab$_2$−GO conjugate (curve a), whereas no signal could be detected on the GO−COOH (curve b). This typical binding energy of amide nitrogen atoms (HN−C═O) indicated successful functionalization of GO to form the HRP−p53^{392}Ab$_2$−GO conjugate. The resulting HRP−p53^{392}Ab$_2$−GO was further characterized by UV−vis spectroscopy, as shown in Figure 3B. For pure p53^{392}Ab$_2$ and HRP, they displayed

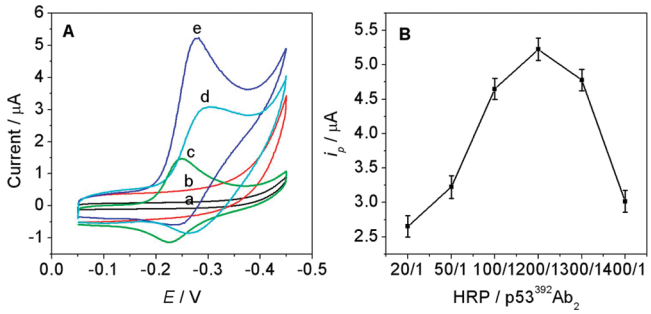

Figure 4. (A) Cyclic voltammograms obtained at (a) AuNPs−SPCE, (b) Ab$_1$/NHS/AuNPs−SPCE in pH 7.4 PBS, (c) Ab$_1$/NHS/AuNPs−SPCE, (d) HRP−streptavidin−biotin−p53^{392}Ab$_2$/phospho-p53^{392}/Ab$_1$/NHS/AuNPs−SPCE, (e) HRP−p53^{392}Ab$_2$−GO/phospho-p53^{392}/Ab$_1$/NHS/AuNPs−SPCE in pH 7.4 PBS containing 25 μM thionine and 2 mM H_2O_2. (B) Effect of HRP/p53^{392}Ab$_2$ ratio on response current. A concentration of 1 ng mL^{-1} phospho-p53^{392} antigen was used during the incubation process.

absorption peaks at 282 nm (curve a) and 404 nm (curve b), respectively. No absorption peak was observed for the GO (curve c). When p53^{392}Ab$_2$ and HRP were bound to GO via the EDC/NHS method, two obvious absorption peaks were observed on the resulting HRP−p53^{392}Ab$_2$−GO conjugate (curve d), indicating successful binding of p53^{392}Ab$_2$ and HRP to GO.

Signal Amplification Immunoassay with HRP−p53^{392}Ab$_2$−GO Conjugate. To enhance detection sensitivity, herein we pursued a multienzyme labeling strategy instead of a single-enzyme label during the immunoassay. For the immunosensor fabrication, phospho-p53^{392} capture antibody (Ab$_1$) was firstly attached onto AuNPs-modified SPCE (AuNPs−SPCE) through a layer of *N*-hydroxysuccinimide-activated hexa(ethylene glycol) undecane thiol (NHS). As shown in Figure 4A, the cyclic voltammograms at AuNPs−SPCE (curve a) and Ab$_1$/NHS/AuNPs−SPCE (curve b) did not show any detectable signal in pH 7.4 PBS. Upon adding 25 μM thionine and 2 mM H_2O_2 to the PBS buffer, the cyclic voltammogram at Ab$_1$/NHS/AuNPs−SPCE exhibited a pair of stable and well-defined redox peaks at −0.225 and −0.247 V (curve c), respectively, which correspond to the electrochemical oxidation and reduction of thionine. When the immunosensor was incubated with 1 ng mL^{-1} phospho-p53^{392} antigen, no obvious change in response was observed at the sensor (data not shown). However, after incubating with biotin−p53^{392}Ab$_2$ for 1 h and then streptavidin−HRP for 20 min, the resulting HRP−streptavidin−biotin−p53^{392}Ab$_2$/phospho-p53^{392}/Ab$_1$/NHS/AuNPs−SPCE displayed an obvious increase in electrocatalytic reduction current (curve d) because of the introduction of HRP onto the electrode surface by the immunoreactions. Furthermore, we observed a more significant increased reduction current at the immunosensor (curve e) when replacing HRP−streptavidin−biotin−p53^{392}Ab$_2$ with the HRP−p53^{392}Ab$_2$−GO conjugate during the sandwich immunoreactions. It is not surprising that the multienzyme labeling strategy enhanced detection responses compared with single-enzyme-labeled antibody in the conventional immunoassay. The achieved amplification of signal was ascribed to a large amount of enzymes loaded on the GO nanocarrier.

Because of the coimmobilization of enzymes and antibodies on the GO nanocarrier, the ratio of HRP and p53^{392}Ab$_2$ (HRP/p53^{392}Ab$_2$) is the most important factor on the response signal. As shown in Figure 4B, one can see that the electrocatalytic current increases with increasing the ratio of HRP/p53^{392}Ab$_2$, and the maximum response is achieved at the ratio of 200/1. The increase of the

dx.doi.org/10.1021/ac101715s |*Anal. Chem.* 2011, 83, 746–752

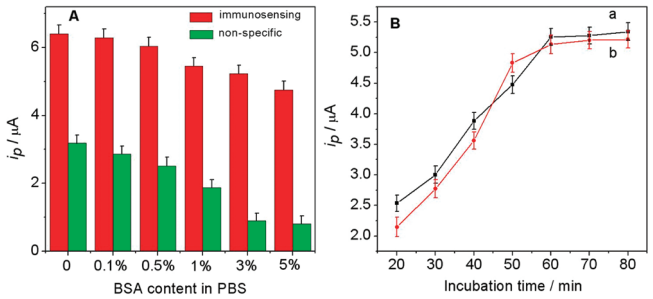

Figure 5. (A) Effect of the concentration of BSA on SWV peak currents of (red bars) HRP−p53^{392}Ab$_2$−GO/phospho-p53^{392}/Ab$_1$/NHS/AuNPs−SPCE and (green bars) HRP−p53^{392}Ab$_2$−GO/Ab$_1$/NHS/AuNPs−SPCE control. (B) Incubation time for (a) capturing phopho-p53^{392} antigen and (b) recognizing HRP−p53^{392}Ab$_2$−GO on the electrochemical responses.

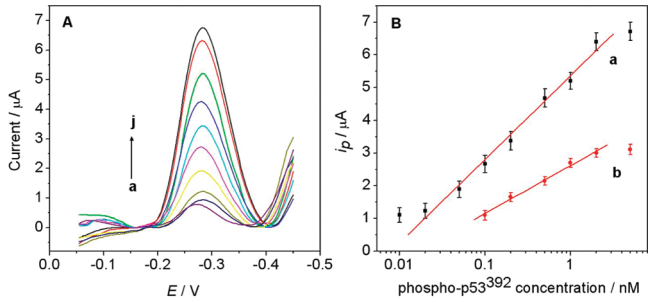

Figure 6. (A) SWV curves acquired at HRP−p53^{392}Ab$_2$−GO/phospho-p53^{392}/Ab$_1$/NHS/AuNPs−SPCE after incubation with (a) 0, (b) 0.01, (c) 0.02, (d) 0.05, (e) 0.1, (f) 0.2, (g) 0.5, (h) 1, (i) 2, and (j) 5 ng mL^{-1} phospho-p53^{392} antigen in pH 7.4 PBS containing 25 μM thionine and 2 mM H_2O_2. (B) Calibration plots of the (a) proposed HRP−p53^{392}Ab$_2$−GO/phospho-p53^{392}/Ab$_1$/NHS/AuNPs−SPCE and (b) traditional HRP−streptavidin−biotin−p53^{392}Ab$_2$/phospho-p53^{392}/Ab$_1$/NHS/AuNPs−SPCE for detecting phospho-p53^{392} antigen.

HRP/p53^{392}Ab$_2$ ratio could increase the total amount of HRP loaded per GO nanocarrier, which is expected to enhance the response amplification for this sandwich immunoassay. However, the reducing amount of p53^{392}Ab$_2$ in the immunoassay may decrease immunocoupling efficiency to the captured phospho-p53^{392} antigen at the electrode surface, which may result in a decreased response. Therefore, the HRP/p53^{392}Ab$_2$ ratio of 200/1 is selected as the optimal condition to prepare the HRP−p53^{392}Ab$_2$−GO conjugate.

To determine the amount of active HRP in the HRP−p53^{392}Ab$_2$−GO conjugate dispersion, the mixture was reacted with HRP substrate TMB. The reaction product was read at 650 nm. These results were compared to a standard curve constructed with pure HRP by an enzyme activity experiment. The concentration of active HRP in the HRP−p53^{392}Ab$_2$−GO conjugate dispersion was determined to be 4.77 μg mL^{-1}.

Optimization of Detection Conditions. Nonspecific adsorption has a significant influence on immunoassay responses. A series of corresponding control experiments (Ab$_1$/NHS/AuNPs−SPCE was directly exposed to HRP−p53^{392}Ab$_2$−GO conjugate in the absence of phospho-p53^{392} antigen) using different concentrations of BSA blocking were performed in PBS containing thionine and H_2O_2 by SWV measurements. As shown in Figure 5A, the current responses at both the HRP−p53^{392}Ab$_2$−GO/phospho-p53^{392}/Ab$_1$/NHS/AuNPs−SPCE and corresponding control HRP−p53^{392}Ab$_2$−GO/Ab$_1$/NHS/AuNPs−SPCE decreased upon increasing the concentrations of BSA blocking agent due to the shield effect of BSA. The minimization of the nonspecific adsorption (corresponding control signals) was achieved at 3% BSA in PBS and tended to be stable after that; however, the immunsensing signals continue to decrease obviously when raising the BSA concentration to 5%. The decrease of signal may be due to the steric hindrance of large molecules, which block or hinder the diffusion of substrate toward the electrode surface and the electron-transfer reaction. Although the immunosensor displayed much higher electrochemical responses at very low BSA concentration (0.1%), the nonspecific signal was very high. Considering the sensitivity of the electrochemical response to quantify phospho-p53^{392} antigen and limiting the nonspecific adsorption, 3% BSA in PBS was selected as the blocking agent.

The incubation time is another important parameter for both capturing phopho-p53^{392} antigen and specifically recognizing HRP−p53^{392}Ab$_2$−GO. It can be seen that the electrochemical response increases with increasing incubation time of phospho-p53^{392} antigen and tends to a steady value after 1 h (curve a in Figure 5B), indicating a thorough capturing of the antigens on the electrode surface. In the second immunoassay incubation step, the catalytic current also increases upon increasing the incubation time and reaches a plateau at 1 h, which shows saturated binding sites between antigen and detection antibody (curve b in Figure 5B). A longer time incubation could result in a large nonspecific signal. Therefore, the optimal incubation time for the first and second immunoreactions is 1 h, respectively.

Analytical Performance of the Immunosensor for Electrochemical Detection of Phospho-p53^{392} Antigen. After the above optimizations, the proposed immunosensor using HRP−p53^{392}Ab$_2$−GO conjugate in the amplification approach is challenged with different concentrations of phospho-p53^{392}, as shown in Figure 6A. It can be seen that the SWV currents increase with the increase of phospho-p53^{392} concentrations. The linear response is obtained over the concentration range from 0.02 to 2 nM with the detection limit of 0.01 nM (curve a in Figure 6B). Comparably, we used the traditional HRP−streptavidin−biotin−p53^{392}Ab$_2$ for phospho-p53^{392} determination on electrode. The increase of reduction current is also proportional to the phospho-p53^{392} concentration in the range of 0.1−2 nM with the detection limit of 0.1 nM (curve b in Figure 6B). It reveals that the proposed multienzyme labeling amplification strategy using GO as a nanocarrier possesses the advantages of both higher sensitivity and wider linear range than that of the traditional labeling immunoassay. The detection limit of this immunosensor is 10-fold lower than that of a conventional sensor with the HRP−streptavidin−biotin−p53^{392}Ab$_2$ label. The achieved high sensitivity mainly results from the excessive enzymes present in the GO. The phospho-p53 (S392) ELISA kit shows a linear range from 0.05 to 3 nM with detection limit of 0.05 nM for phospho-p53^{392}. This amplified electrochemical immunosensor is more sensitive than that of the ELISA results. Moreover, the electrochemical detector used in this work is much simpler and lower in cost compared with the instrument used in the ELISA kit.

To further investigate the selectivity and validate the sensor performance for phospho-p53^{392} detection, the proposed immunosensor was tested using human plasma as matrix. The immunosensor was incubated in human plasma samples spiked with 1.0 ng mL^{-1} phospho-p53^{392} and different possible interfering agents such as p53, phospho-p53^{15}, and phospho-p53^{46}. No remarkable electrochemical response change was observed for the mixed sample in comparison to the result obtained only in the presence of phospho-p53^{392}, indicating good selectivity for determination of phospho-p53^{392}.

dx.doi.org/10.1021/ac101715s |*Anal. Chem.* 2011, 83, 746–752

Table 1. Recovery Results from the Immunosensor for Different Concentrations of Phospho-p53^{392} Spiked in Human Plasma

sample no.	1	2	3	4	5
spiked (nM)	0.05	0.10	0.20	0.50	1.0
immunosensor (nM)	0.046 ± 0.002	0.096 ± 0.003	0.207 ± 0.005	0.519 ± 0.004	1.013 ± 0.006
recovery (%)	92.0	96.0	103.5	103.8	101.3

The reproducibility of the proposed immunosensor is evaluated by intra- and interassay coefficients of variation (CVs). The intra-assay precision of the analytical method is evaluated by analyzing one immunosensor for six replicate determinations. The CVs of the intra-assay were 3.3% and 4.6% at 0.1 and 1.0 ng mL^{-1} phospho-p53^{392}, respectively. Similarly, the interassay CVs on six immunosensors were 3.9% and 5.7% at 0.1 and 1.0 ng mL^{-1} phospho-p53^{392}, respectively. These results demonstrated acceptable reproducibility and precision of the proposed immunosensor. In addition, the immunosensor could be stored at 4 °C. In this way, over 90% of the initial response remained after 1 week and 80% of the initial response remained after 1 month, indicating acceptable stability.

A series of phospho-p53^{392} human plasma samples were used to test the accuracy of the electrochemical quantification approach. Phospho-p53^{392} human plasma samples were prepared by spiking different amounts of phospho-p53^{392} with known concentrations to human plasma. The results are summarized in Table 1, which shows the recoveries are in the range of 92−104%, indicating that the electrochemical immunosensing approach is reliable.

CONCLUSIONS

In summary, we have successfully designed a multienzyme labeling GO strategy in a signal amplification procedure and demonstrated its use in the ultrasensitive, selective, and accurate quantification of phospho-p53^{392} by electrochemical immunoassay. Enhanced sensitivity is achieved by using functionalized GO as a nanocarrier to link enzyme and signal antibody at high ratio. The proposed immunosensor shows excellent performance for detection of phosphorylated protein with a wide linear range and low detection limit and acceptable stability, reproducibility, and accuracy. We anticipate that this method can be extended for determination of other proteins and provide a promising potential in clinical applications.

AUTHOR INFORMATION

Corresponding Author

*E-mail: yuehe.lin@pnl.gov.

ACKNOWLEDGMENT

The work was done at Pacific Northwest National Laboratory (PNNL) and was supported partially by the National Institutes of Health CounterACT program through the National Institute of Neurological Disorders and Stroke (award no. NS058161-01) and a PNNL Laboratory Directed Research and Development program. Its contents are solely the responsibility of the authors and do not necessarily represent the official views of the federal government. PNNL is operated for the U.S. Department of Energy (DOE) by Battelle under contract DE-AC05-76RL01830. The materials characterization was performed at the Environmental Molecular Sciences Laboratory, a national scientific user facility sponsored by DOE's office of Biological and Environmental Research located at PNNL. Dan Du acknowledges the support from the National Natural Science Foundation of China (21075047) and the Program for Chenguang Young Scientist for Wuhan (200950431184).

REFERENCES

(1) Toledo, F; Wahl, G. M. *Nat. Rev. Cancer* **2006,** *6,* 909–923.
(2) Evan, G. I.; Vousden, K. H. *Nature* **2001,** *411,* 342–348.
(3) Ko, L. J.; Prives, C. *Genes Dev.* **1996,** *10,* 1054–1072.
(4) Appella, E.; Anderson, C. W. *Eur. J. Biochem.* **2001,** *268,* 2764–2772.
(5) Bode, A. M.; Dong, Z. *Nat. Rev. Cancer* **2004,** *4,* 793–805.
(6) Minamoto, T.; Buschmann, T.; Habelhah, H.; Matusevich, E.; Tahara, H.; Boerresen-Dale, A.; Harris, C.; Sidransky, D.; Ronai, Z. *Oncogene* **2001,** *20,* 3341–3347.
(7) Bar, J. K.; Słomska, I.; Rabczyńki, J.; Noga, L.; Gryboś, M. *Int. J Gynecol. Cancer* **2009,** *19,* 1322–1328.
(8) Matsumoto, M.; Furihata, M.; Ohtsuki, Y. *Med. Mol. Morphol.* **2006,** *39,* 79–87.
(9) Furihata, M.; Kurabayashl, A.; Matsumoto, M.; Sonobe, H.; Ohtsuki, Y.; Terao, N.; Kuwahara, M.; Shuin, T. *J. Pathol.* **2002,** *197,* 82–88.
(10) Yap, D. B. S.; Hsieh, J. K.; Zhong, S.; Heath, V.; Gusterson, B.; Crook, T.; Lu, X. *Cancer Res.* **2004,** *64,* 4749–4754.
(11) Matsumoto, M.; Furihata, M.; Kurabayashi, A.; Sasaguri, S.; Araki, K.; Hayashi, H.; Ohtsuki, Y. *Oncology* **2004,** *67,* 143–150.
(12) Pühringer-Oppermann, F.; Stahl, M.; Keller, G.; Sarbia, M. *J. Cancer Res. Clin. Oncol.* **2006,** *132,* 433–438.
(13) Tichy, A.; Zaškodova, D.; Zoelzer, F.; Vavrova, J.; Šinkorova, Z.; Pejchal, J.; Osterreicher, J.; Řezačova, M. *Folia Biol.* **2009,** *55,* 41–44.
(14) Cox, M. L.; Meek, D. W. *Cell. Signalling* **2010,** *22,* 564–571.
(15) Wu, J.; Fu, Z. F.; Yan, F.; Ju, H. X. *Trends Anal. Chem.* **2007,** *26,* 679–688.
(16) Sánchez, S.; Roldán, M.; Pérez, S.; Fàbregas, E. *Anal. Chem.* **2008,** *80,* 6508–6514.
(17) Das, J.; Aziz, M. A.; Yang, H. *J. Am. Chem. Soc.* **2006,** *128,* 16022–16023.
(18) (a) Hazarika, P.; Ceyhan, B.; Niemeyer, C. M. *Small* **2005,** *1,* 844–848. (b) Liu, G.; Lin, Y. *Talanta* **2007,** *74,* 308–317.
(19) Liu, G.; Lin, Y. Y.; Wang, J.; Wu, H.; Wai, C. M.; Lin, Y. *Anal. Chem.* **2007,** *79,* 7644–7653.
(20) Wang, J.; Liu, G. D.; Engelhard, M. H.; Lin, Y. H. *Anal. Chem.* **2006,** *78,* 6974–6979.
(21) Wang, J.; Liu, G. D.; Lin, Y. H. *Small* **2006,** *2,* 1134–1138.
(22) Cui, R. J.; Liu, C.; Shen, J. M.; Gao, D.; Zhu, J. J.; Chen, H. Y. *Adv. Funct. Mater.* **2008,** *18,* 2197–2204.
(23) Jie, G.; Huang, H.; Sun, X.; Zhu, J. J. *Biosens. Bioelectron.* **2008,** *23,* 1896–1899.
(24) Yu, X.; Munge, B.; Patel, V.; Jensen, G.; Bhirde, A.; Gong, J. D.; Kim, S. N.; Gillespie, J.; Gutkind, J. S.; Papadimitrakopoulos, F.; Rusling, J. F. *J. Am. Chem. Soc.* **2006,** *128,* 11199–11205.
(25) Malhotra, R.; Patel, V.; Vaque, J. P.; Gutkind, J. S.; Rusling, J. F. *Anal. Chem.* **2010,** *82,* 3118–3123.
(26) Du, D.; Zou, Z. X.; Shin, Y.; Wang, J.; Wu, H.; Engelhard, M. H.; Liu, J.; Aksay, I. A.; Lin, Y. H. *Anal. Chem.* **2010,** *82,* 2989–2995.
(27) Lai, G. S.; Yan, F.; Ju, H. X. *Anal. Chem.* **2009,** *81,* 9730–9736.
(28) Wu, Y. F.; Chen, C. L.; Liu, S. Q. *Anal. Chem.* **2009,** *81,* 1600–1607.
(29) Mani, V.; Chikkaveeraiah, B. V.; Patel, V.; Gutkind, J. S.; Rusling, J. F. *ACS Nano* **2009,** *3,* 585–594.
(30) Geim, A. K.; Novoselov, K. S. *Nat. Mater.* **2007,** *6,* 183–191.

(31) Kopelevich, Y.; Esquinazi, P. *Adv. Mater.* **2007,** *19*, 4559–4563.
(32) Li, X. L.; Wang, X. R.; Zhang, L.; Lee, S.; Dai, H. J. *Science* **2008,** *319*, 1229–1232.
(33) Stankovich, S.; Dikin, D. A.; Dommett, G. H. B.; Kohlhaas, K. M.; Zimney, E. J.; Stach, E. A.; Piner, R. D.; Nguyen, S. T.; Ruoff, R. S. *Nature* **2006,** *442*, 282–286.
(34) Shao, Y. Y.; Wang, J.; Wu, H.; Liu, J.; Aksay, I. A.; Lin, Y. H. *Electroanalysis* **2010,** *22*, 1027–1036.
(35) Tang, Z. W.; Wu, H.; Cort, J. R.; Buchko, G. W.; Zhang, Y. Y.; Shao, Y. Y.; Aksay, I. A.; Liu, J.; Lin, Y. H. *Small* **2010,** *6*, 1205–1209.
(36) Wang, Y.; Shao, Y. Y.; Matson, D. W.; Li, J. H.; Lin, Y. H. *ACS Nano* **2010,** *4*, 1790–1798.
(37) Zhang, H.; Lv, X. J.; Li, Y. M.; Wang, Y.; Li, J. H. *ACS Nano* **2010,** *4*, 380–386.
(38) Sun, X. M.; Liu, Z.; Welsher, K.; Robinson, J. T.; Goodwin, A.; Zaric, S.; Dai, H. J. *Nano Res.* **2008,** *1*, 203–212.
(39) Liu, Z.; Robinson, J. T.; Sun, X.; Dai, H. J. *J. Am. Chem. Soc.* **2008,** *130*, 10876–10877.
(40) Yang, X. Y.; Zhang, X. Y.; Liu, Z. F.; Ma, Y. F.; Huang, Y.; Chen, Y. S. *J. Phys. Chem. C* **2008,** *112*, 17554–17558.
(41) Zhang, L. M.; Xia, J. G.; Zhao, Q. H.; Liu, L. W.; Zhang, Z. J. *Small* **2010,** *6*, 537–544.
(42) Gilje, S.; Han, S.; Wang, M.; Wang, K. L.; Kaner, R. B. *Nano Lett.* **2007,** *7*, 3394–3398.
(43) Eda, G.; Fanchini, G.; Chhowalla, M. *Nat. Nanotechnol.* **2008,** *3*, 270–274.
(44) Shao, Y. Y.; Wang, J.; Engelhard, M.; Wang, C. M.; Lin, Y. H. *J. Mater. Chem.* **2010,** *20*, 743–748.
(45) Szabó, T.; Berkesi, O.; Forgó, P.; Josepovits, K.; Sanakis, Y.; Petridis, D.; Dékány, I. *Chem. Mater.* **2006,** *18*, 2740–2749.
(46) Dikin, D. A.; Stankovich, S.; Zimney, E. J.; Piner, R. D.; Dommett, G. H. B.; Evmenenko, G.; Nguyen, S. T.; Ruoff, R. S. *Nature* **2007,** *448*, 457–460.
(47) McAllister, M. J.; Li, J. L.; Adamson, D. H.; Schniepp, H. C.; Abdala, A. A.; Liu, J.; Herrera-Alonso, M.; Milius, D. L.; Car, R.; Prud'homme, R. K.; Aksay, I. A. *Chem. Mater.* **2007,** *19*, 4396–4404.